PHYSICAL REVIEW D **84**, 091102(R) (2011)

Search for η_c' decays into vector meson pairs

M. Ablikim,[1] M. N. Achasov,[5] D. Alberto,[40] F. F. An,[1] Q. An,[38] Z. H. An,[1] J. Z. Bai,[1] R. Baldini,[19] Y. Ban,[25] J. Becker,[2] N. Berger,[1] M. Bertani,[19] J. M. Bian,[1] E. Boger,[17,*] O. Bondarenko,[18] I. Boyko,[17] R. A. Briere,[3] V. Bytev,[17] X. Cai,[1] A. C. Calcaterra,[19] G. F. Cao,[1] J. F. Chang,[1] G. Chelkov,[17,*] G. Chen,[1] H. S. Chen,[1] J. C. Chen,[1] M. L. Chen,[1] S. J. Chen,[23] Y. Chen,[1] Y. B. Chen,[1] H. P. Cheng,[13] Y. P. Chu,[1] D. Cronin-Hennessy,[37] H. L. Dai,[1] J. P. Dai,[1] D. Dedovich,[17] Z. Y. Deng,[1] I. Denysenko,[17,†] M. Destefanis,[40] Y. Ding,[21] L. Y. Dong,[1] M. Y. Dong,[1] S. X. Du,[43] J. Fang,[1] S. S. Fang,[1] C. Q. Feng,[38] C. D. Fu,[1] J. L. Fu,[23] Y. Gao,[34] C. Geng,[38] K. Goetzen,[7] W. X. Gong,[1] M. Greco,[40] M. H. Gu,[1] Y. T. Gu,[9] Y. H. Guan,[6] A. Q. Guo,[24] L. B. Guo,[22] Y. P. Guo,[24] Y. L. Han,[1] X. Q. Hao,[1] F. A. Harris,[36] K. L. He,[1] M. He,[1] Z. Y. He,[24] Y. K. Heng,[1] Z. L. Hou,[1] H. M. Hu,[1] J. F. Hu,[6] T. Hu,[1] B. Huang,[1] G. M. Huang,[14] J. S. Huang,[11] X. T. Huang,[27] Y. P. Huang,[1] T. Hussain,[39] C. S. Ji,[38] Q. Ji,[1] X. B. Ji,[1] X. L. Ji,[1] L. K. Jia,[1] L. L. Jiang,[1] X. S. Jiang,[1] J. B. Jiao,[27] Z. Jiao,[13] D. P. Jin,[1] S. Jin,[1] F. F. Jing,[34] N. Kalantar-Nayestanaki,[18] M. Kavatsyuk,[18] W. Kuehn,[35] W. Lai,[1] J. S. Lange,[35] J. K. C. Leung,[33] C. H. Li,[1] Cheng Li,[38] Cui Li,[38] D. M. Li,[43] F. Li,[1] G. Li,[1] H. B. Li,[1] J. C. Li,[1] K. Li,[10] Lei Li,[1] N. B. Li,[22] Q. J. Li,[1] S. L. Li,[1] W. D. Li,[1] W. G. Li,[1] X. L. Li,[27] X. N. Li,[1] X. Q. Li,[24] X. R. Li,[26] Z. B. Li,[31] H. Liang,[38] Y. F. Liang,[29] Y. T. Liang,[35] X. T. Liao,[1] B. J. Liu,[32] C. L. Liu,[3] C. X. Liu,[1] C. Y. Liu,[1] F. H. Liu,[28] Fang Liu,[1] Feng Liu,[14] H. Liu,[1] H. B. Liu,[6] H. H. Liu,[12] H. M. Liu,[1] H. W. Liu,[1] J. P. Liu,[41] K. Liu,[25] K. Liu,[6] K. Y. Liu,[21] Q. Liu,[36] S. B. Liu,[38] X. Liu,[20] X. H. Liu,[1] Y. B. Liu,[24] Y. W. Liu,[38] Yong Liu,[1] Z. A. Liu,[1] Zhiqiang Liu,[1] Zhiqing Liu,[1] H. Loehner,[18] G. R. Lu,[11] H. J. Lu,[13] J. G. Lu,[1] Q. W. Lu,[28] X. R. Lu,[6] Y. P. Lu,[1] C. L. Luo,[22] M. X. Luo,[42] T. Luo,[36] X. L. Luo,[1] M. Lv,[1] C. L. Ma,[6] F. C. Ma,[21] H. L. Ma,[1] Q. M. Ma,[1] S. Ma,[1] T. Ma,[1] X. Ma,[1] X. Y. Ma,[1] M. Maggiora,[40] Q. A. Malik,[39] H. Mao,[1] Y. J. Mao,[25] Z. P. Mao,[1] J. G. Messchendorp,[18] J. Min,[1] T. J. Min,[1] R. E. Mitchell,[16] X. H. Mo,[1] N. Yu. Muchnoi,[5] Y. Nefedov,[17] I. B. Nikolaev,[5] Z. Ning,[1] S. L. Olsen,[26] Q. Ouyang,[1] S. Pacetti,[19] J. W. Park,[26] M. Pelizaeus,[36] K. Peters,[7] J. L. Ping,[22] R. G. Ping,[1] R. Poling,[37] C. S. J. Pun,[33] M. Qi,[23] S. Qian,[1] C. F. Qiao,[6] X. S. Qin,[1] J. F. Qiu,[1] K. H. Rashid,[39] G. Rong,[1] X. D. Ruan,[9] A. Sarantsev,[17,‡] J. Schulze,[2] M. Shao,[38] C. P. Shen,[36,§] X. Y. Shen,[1] H. Y. Sheng,[1] M. R. Shepherd,[16] X. Y. Song,[1] S. Spataro,[40] B. Spruck,[35] D. H. Sun,[1] G. X. Sun,[1] J. F. Sun,[11] S. S. Sun,[1] X. D. Sun,[1] Y. J. Sun,[38] Y. Z. Sun,[1] Z. J. Sun,[1] Z. T. Sun,[38] C. J. Tang,[29] X. Tang,[1] H. L. Tian,[1] D. Toth,[37] G. S. Varner,[36] B. Wang,[9] B. Q. Wang,[25] K. Wang,[1] L. L. Wang,[4] L. S. Wang,[1] M. Wang,[27] P. Wang,[1] P. L. Wang,[1] Q. Wang,[1] Q. J. Wang,[1] S. G. Wang,[25] X. L. Wang,[38] Y. D. Wang,[38] Y. F. Wang,[1] Y. Q. Wang,[27] Z. Wang,[1] Z. G. Wang,[1] Z. Y. Wang,[1] D. H. Wei,[8] Q. G. Wen,[38] S. P. Wen,[1] U. Wiedner,[2] L. H. Wu,[1] N. Wu,[1] W. Wu,[21] Z. Wu,[1] Z. J. Xiao,[22] Y. G. Xie,[1] Q. L. Xiu,[1] G. F. Xu,[1] G. M. Xu,[25] H. Xu,[1] Q. J. Xu,[10] X. P. Xu,[30] Y. Xu,[24] Z. R. Xu,[38] Z. Z. Xu,[38] Z. Xue,[1] L. Yan,[38] W. B. Yan,[38] Y. H. Yan,[15] H. X. Yang,[1] T. Yang,[9] Y. Yang,[14] Y. X. Yang,[8] H. Ye,[1] M. Ye,[1] M. H. Ye,[4] B. X. Yu,[1] C. X. Yu,[24] S. P. Yu,[27] C. Z. Yuan,[1] W. L. Yuan,[22] Y. Yuan,[1] A. A. Zafar,[39] A. Zallo,[19] Y. Zeng,[15] B. X. Zhang,[1] B. Y. Zhang,[1] C. Zhang,[23] C. C. Zhang,[1] D. H. Zhang,[1] H. H. Zhang,[31] H. Y. Zhang,[1] J. Zhang,[22] J. Q. Zhang,[1] J. W. Zhang,[1] J. Y. Zhang,[1] J. Z. Zhang,[1] L. Zhang,[23] S. H. Zhang,[1] T. R. Zhang,[22] X. J. Zhang,[1] X. Y. Zhang,[27] Y. Zhang,[1] Y. H. Zhang,[1] Y. S. Zhang,[9] Z. P. Zhang,[38] Z. Y. Zhang,[41] G. Zhao,[1] H. S. Zhao,[1] Jiawei Zhao,[38] Jingwei Zhao,[1] Lei Zhao,[38] Ling Zhao,[1] M. G. Zhao,[24] Q. Zhao,[1] S. J. Zhao,[43] T. C. Zhao,[1] X. H. Zhao,[23] Y. B. Zhao,[1] Z. G. Zhao,[38] Z. L. Zhao,[9] A. Zhemchugov,[17,*] B. Zheng,[1] J. P. Zheng,[1] Y. H. Zheng,[6] Z. P. Zheng,[1] B. Zhong,[1] J. Zhong,[2] L. Zhong,[34] L. Zhou,[1] X. K. Zhou,[6] X. R. Zhou,[38] C. Zhu,[1] K. Zhu,[1] K. J. Zhu,[1] S. H. Zhu,[1] X. L. Zhu,[34] X. W. Zhu,[1] Y. S. Zhu,[1] Z. A. Zhu,[1] J. Zhuang,[1] B. S. Zou,[1] J. H. Zou,[1] and J. X. Zuo[1]

(BESIII Collaboration)

[1]*Institute of High Energy Physics, Beijing 100049, P. R. China*
[2]*Bochum Ruhr-University, 44780 Bochum, Germany*
[3]*Carnegie Mellon University, Pittsburgh, Pennsylvania 15213, USA*
[4]*China Center of Advanced Science and Technology, Beijing 100190, P. R. China*
[5]*G. I. Budker Institute of Nuclear Physics SB RAS (BINP), Novosibirsk 630090, Russia*
[6]*Graduate University of Chinese Academy of Sciences, Beijing 100049, P. R. China*
[7]*GSI Helmholtzcentre for Heavy Ion Research GmbH, D-64291 Darmstadt, Germany*
[8]*Guangxi Normal University, Guilin 541004, P. R. China*
[9]*Guangxi University, Naning 530004, P. R. China*
[10]*Hangzhou Normal University, Hangzhou 310036, P. R. China*
[11]*Henan Normal University, Xinxiang 453007, P. R. China*
[12]*Henan University of Science and Technology, Luoyang 471003, P. R. China*
[13]*Huangshan College, Huangshan 245000, P. R. China*

1550-7998/2011/84(9)/091102(7)

[14]Huazhong Normal University, Wuhan 430079, P. R. China
[15]Hunan University, Changsha 410082, P. R. China
[16]Indiana University, Bloomington, Indiana 47405, USA
[17]Joint Institute for Nuclear Research, 141980 Dubna, Russia
[18]KVI/University of Groningen, 9747 AA Groningen, The Netherlands
[19]Laboratori Nazionali di Frascati—INFN, 00044 Frascati, Italy
[20]Lanzhou University, Lanzhou 730000, P. R. China
[21]Liaoning University, Shenyang 110036, P. R. China
[22]Nanjing Normal University, Nanjing 210046, P. R. China
[23]Nanjing University, Nanjing 210093, P. R. China
[24]Nankai University, Tianjin 300071, P. R. China
[25]Peking University, Beijing 100871, P. R. China
[26]Seoul National University, Seoul, 151-747 Korea
[27]Shandong University, Jinan 250100, P. R. China
[28]Shanxi University, Taiyuan 030006, P. R. China
[29]Sichuan University, Chengdu 610064, P. R. China
[30]Soochow University, Suzhou 215006, China
[31]Sun Yat-Sen University, Guangzhou 510275, P. R. China
[32]The Chinese University of Hong Kong, Shatin, N. T., Hong Kong
[33]The University of Hong Kong, Pokfulam, Hong Kong
[34]Tsinghua University, Beijing 100084, P. R. China
[35]Universitaet Giessen, 35392 Giessen, Germany
[36]University of Hawaii, Honolulu, Hawaii 96822, USA
[37]University of Minnesota, Minneapolis, Minnesota 55455, USA
[38]University of Science and Technology of China, Hefei 230026, P. R. China
[39]University of the Punjab, Lahore-54590, Pakistan
[40]University of Turin and INFN, Turin, Italy
[41]Wuhan University, Wuhan 430072, P. R. China
[42]Zhejiang University, Hangzhou 310027, P. R. China
[43]Zhengzhou University, Zhengzhou 450001, P. R. China
(Received 6 October 2011; published 29 November 2011)

The processes $\eta_c' \to \rho^0\rho^0$, $K^{*0}\bar{K}^{*0}$, and $\phi\phi$ are searched for using a sample of 1.06×10^8 ψ' events collected with the BESIII detector at the BEPCII collider. No signals are observed in any of the three final states. The upper limits on the decay branching fractions are determined to be $\mathcal{B}(\eta_c' \to \rho^0\rho^0) < 3.1 \times 10^{-3}$, $\mathcal{B}(\eta_c' \to K^{*0}\bar{K}^{*0}) < 5.4 \times 10^{-3}$, and $\mathcal{B}(\eta_c' \to \phi\phi) < 2.0 \times 10^{-3}$ at the 90% confidence level. The upper limits are lower than the existing theoretical predictions.

DOI: 10.1103/PhysRevD.84.091102 PACS numbers: 14.40.Pq, 12.38.Qk, 13.20.Gd, 13.25.Gv

The radially ($n = 2$) excited S-wave spin-singlet charmonium state, η_c', labeled $\eta_c(2S)$, was observed in $B^\pm \to K^\pm \eta_c'$, $\eta_c' \to K_S^0 K^\pm \pi^\mp$ by the Belle Collaboration [1] and was confirmed by the CLEO and *BABAR* collaborations [2]. In addition to the $K\bar{K}\pi$ final state, $\eta_c' \to 3(\pi^+\pi^-)$, $K^+K^-2(\pi^+\pi^-)$, $K_S^0 K^\pm \pi^\mp \pi^+\pi^-$, and $\pi^+\pi^-K^+K^-\pi^0$ are also reported [3]. The production of η_c' is also expected from the radiative magnetic dipole ($M1$) transition of ψ'. The decay $\psi' \to \gamma\eta_c'$, $\eta_c' \to K_S^0 K^+\pi^- +$ c.c. was observed at BESIII [4] with a branching fraction $\mathcal{B}(\psi' \to \gamma\eta_c') = (4.7 \pm 0.9 \pm 3.0) \times 10^{-4}$, confirming the possibility to study η_c' properties in ψ' transitions. In this analysis, we search for the η_c' decaying into vector meson pairs.

The decay modes $\eta_c' \to VV$, where V stands for a light vector meson, are supposed to be highly suppressed by the helicity selection rule [5]. But in Ref. [6], a higher production rate of $\eta_c' \to VV$ is predicted, taking into consideration significant contributions from intermediate charmed meson loops, which provide a mechanism to evade helicity selection rule [7]. The intermediate charmed meson loops can also significantly suppress $\psi' \to VP$ (where P stands for a pseudoscalar meson) strong decay amplitudes [8], which may help to explain the "$\rho\pi$ puzzle" in charmonium decays [9]. The measurement of $\mathcal{B}(\eta_c' \to VV)$ may help in understanding the role played by charmed meson loops in $\eta_c \to VV$.

In this study, an e^+e^- annihilation data sample with $(1.06 \pm 0.04) \times 10^8$ ψ' events [10] is analyzed. Another data sample of 923 pb^{-1} at $\sqrt{s} = 3.773$ GeV is used to estimate non-ψ' background. The data were collected with

*Also at the Moscow Institute of Physics and Technology, Moscow, Russia.
†On leave from the Bogolyubov Institute for Theoretical Physics, Kiev, Ukraine.
‡Also at the PNPI, Gatchina, Russia.
§Now at Nagoya University, Nagoya, Japan.

the BESIII detector which is described in detail elsewhere [11]. A charged-particle tracking system, main drift chamber, is immersed in a 1 T magnetic field. A time-of-flight system and an electromagnetic calorimeter (EMC) surrounding the tracking system are used to identify charged particles and to measure neutral particle energies, respectively. Located outside the EMC, a muon chamber is used to detect muon tracks.

A Monte Carlo (MC) simulation is used to determine the mass resolution and detection efficiency, as well as to study backgrounds. The simulation of the BESIII detector is based on GEANT4 [12], where the interactions of particles with the detector material are simulated. We use the program LUNDCRM [13] to generate inclusive MC events for the background study, where the branching fractions for known decay channels are taken from the Particle Data Group (PDG) [14]. For the signal channel $\psi' \to \gamma\eta_c'$, the photon is generated with the polar angle distribution $1+\cos^2\theta$. To generate the correct decay angle distributions, the $\eta_c' \to VV$ decays are modeled with SVV model [15], and V decays are generated by the VSS model [16], which is used to describe decays of a vector particle into two scalars.

We search for the η_c' in three exclusive decay channels: $\psi' \to \gamma\rho^0\rho^0 \to \gamma 2(\pi^+\pi^-)$, $\psi' \to \gamma K^{*0}\bar{K}^{*0} \to \gamma\pi^+\pi^-K^+K^-$, and $\psi' \to \gamma\phi\phi \to \gamma 2(K^+K^-)$. These final states, denoted as $\psi' \to \gamma X$ hereafter, contain one radiative photon and four charged tracks. The charged tracks are required to pass within 1 cm of the e^+e^- annihilation interaction point transverse to the beam line and within 10 cm of the interaction point along the beam axis. Each track should have good quality in track fitting and satisfy $|\cos\theta| < 0.93$, where θ is the polar angle with respect to the e^+ beam direction. Reconstructed events are required to have four charged tracks and zero net charge. Information from dE/dx and time-of-flight is used for charged-particle identification (PID), and $\chi^2_{\rm PID}(i)$ is calculated for each charged track, where i is the corresponding charged-particle hypothesis including pion, kaon, and proton. For a specific decay channel, the total $\chi^2_{\rm PID}$ is obtained by summing $\chi^2_{\rm PID}(i)$ over the charged tracks. There is a loop to match the charged tracks to the final state particles in the decay channel, and the matching with the minimum $\chi^2_{\rm PID}$ is adopted. The decay channel for a reconstructed event is selected as the one with the minimum $\chi^2_{\rm PID}$ among possible decay channels. Photons are reconstructed by clustering EMC crystal energies with a minimum energy of 25 MeV. The photon candidates are required to be detected in the active area of the EMC ($|\cos\theta_\gamma| < 0.8$ for the barrel and $0.86 < |\cos\theta_\gamma| < 0.92$ for the endcaps). Timing requirements are used in the EMC to suppress electronic noise and energy deposits unrelated to the event.

In order to reduce background from non-VV production, the invariant masses of the final decay particles are required to satisfy $0.67\ \mathrm{GeV}/c^2 < M_{\pi^+\pi^-} < 0.87\ \mathrm{GeV}/c^2$, $0.85\,\mathrm{GeV}/c^2 < M_{\pi^\pm K^\mp} < 0.95\,\mathrm{GeV}/c^2$, and $1.01\,\mathrm{GeV}/c^2 < M_{K^+K^-} < 1.03\,\mathrm{GeV}/c^2$, for ρ^0, K^{*0}, and ϕ candidates, respectively, which are determined by fitting their mass distributions in the χ_{cJ} mass region. Here the background level has been considered in the choice of the selection criterion for each channel. The ratios of signal over non-V background are near 1 at the edges of the mass selection region for ρ^0 and K^{*0}.

A kinematic fit is performed to improve the mass resolution and reject backgrounds. The four-momenta of the charged tracks and the photon candidate are constrained to the initial ψ' four-momentum ($4C$ fit). When there is more than one photon, the photon with the minimum χ^2 from the $4C$ fit, χ^2_{4C}, is taken as the radiative photon, and χ^2_{4C} is required to be less than 40.

Background from $\psi' \to \pi^+\pi^- J/\psi$ with J/ψ decaying into a lepton pair is removed by requiring the recoil mass [17] of any $\pi^+\pi^-$ pair to be below the J/ψ mass ($m^{\rm recoil}_{\pi^+\pi^-} < 3.05\ \mathrm{GeV}/c^2$). Events from $\psi' \to \eta J/\psi$, with $\eta \to \pi^+\pi^-\pi^0(\gamma)$ and J/ψ decays into lepton pairs, are also removed by this requirement.

The background remaining can be separated into three categories: events with no radiative photon ($\psi' \to X$); events with an extra photon in the final state ($\psi' \to \pi^0 X$, $\pi^0 \to \gamma\gamma$); and events with the same final state as the signal ($\psi' \to \gamma X$), but where the photon comes from initial state radiation or final state radiation (FSR).

The background from $\psi' \to X$ with no radiative photon comes from events where the charged tracks plus a fake photon satisfy the $4C$ kinematic fit. In the X mass spectrum from a $4C$ kinematic fit, this background contributes a peak close to the η_c' mass, around $3.656\ \mathrm{GeV}/c^2$, and decreases sharply at high mass due to the 25 MeV requirement on the photon energy. If the measured energy of the candidate photon is not used in the kinematic fit, thus becoming a $3C$ fit, this background lies around the ψ' mass region ($3.66\ \mathrm{GeV}/c^2 \sim 3.70\ \mathrm{GeV}/c^2$) in the mass spectrum, as the photon energy from the fit tends to be close to zero energy (see Fig. 1). There is little change in the η_c' mass resolution due to one less constraint in the kinematic fit, but the separation of the η_c' signal from the background is much improved. Therefore, the result from the $3C$ fit (M_X^{3C}) is taken as the final mass spectrum.

The background from $\psi' \to \pi^0 X$ is measured from data by reconstructing the π^0 from its decay into two photons. If there are more than two photons, the π^0 candidate is selected as the one with the minimum χ^2 from a $5C$ fit ($4C$ plus a π^0 mass constraint). $\chi^2_{5C} < 30$ is required to veto backgrounds. A MC sample of $\psi' \to \pi^0 X$ is used to determine the efficiency ratio between events passing the $\psi' \to \gamma X$ and $\psi' \to \pi^0 X$ selections. Finally, the efficiency ratio is used to scale the $\psi' \to \pi^0 X$ sample selected from data to obtain the background contamination from $\psi' \to \pi^0 X$ as a function of the X invariant mass. This background, which is described with a Novosibirsk function [18] as shown in Fig. 2,

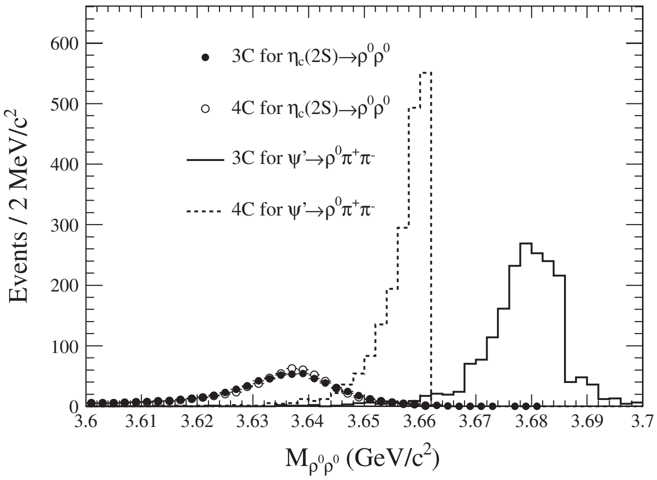

FIG. 1. Comparison between 3C and 4C kinematic fits (unnormalized). Shown in the plot are the signal with the 3C fit (filled circles), signal with the 4C fit (open circles), $\psi' \to X$ background with the 3C fit (solid line), and $\psi' \to X$ background with the 4C fit (dashed line).

contributes a smooth component in the χ_{cJ} ($J=0, 1, 2$) mass region (3.35 GeV$/c^2 \sim 3.60$ GeV$/c^2$), and is almost negligible above 3.60 GeV$/c^2$.

The background shape from $\psi' \to (\gamma_{\rm FSR})X$ is obtained from MC simulation, where the FSR photon is simulated with PHOTOS [19]. The fraction of events with FSR is defined as $R_{\rm FSR} = \frac{N_{\gamma_{\rm FSR}X}}{N_X}$, where $N_{\gamma_{\rm FSR}X}$ (N_X) is the number of events containing an (no) FSR photon that survive selection. This fraction is obtained from measuring the FSR contribution in $\psi' \to \gamma\chi_{c0}$, $\chi_{c0} \to (\gamma_{\rm FSR})X$. The event selection of this FSR sample is very similar to that of the signal mode, except that the reconstructed final state contains two photons, where the softer photon is regarded as the FSR photon. The energy of the FSR photon is not used when performing the 3C kinematic fit for this sample. Events from $\psi' \to \pi^0 X$ are the main background for the FSR sample and are excluded by requiring the invariant mass of the two photons to be outside of the π^0 signal region. Figure 3 shows the two-dimensional distribution of M_X^{3C} versus $M^{3C}_{\gamma_{\rm FSR}X}$. If we add the four-momenta of the FSR

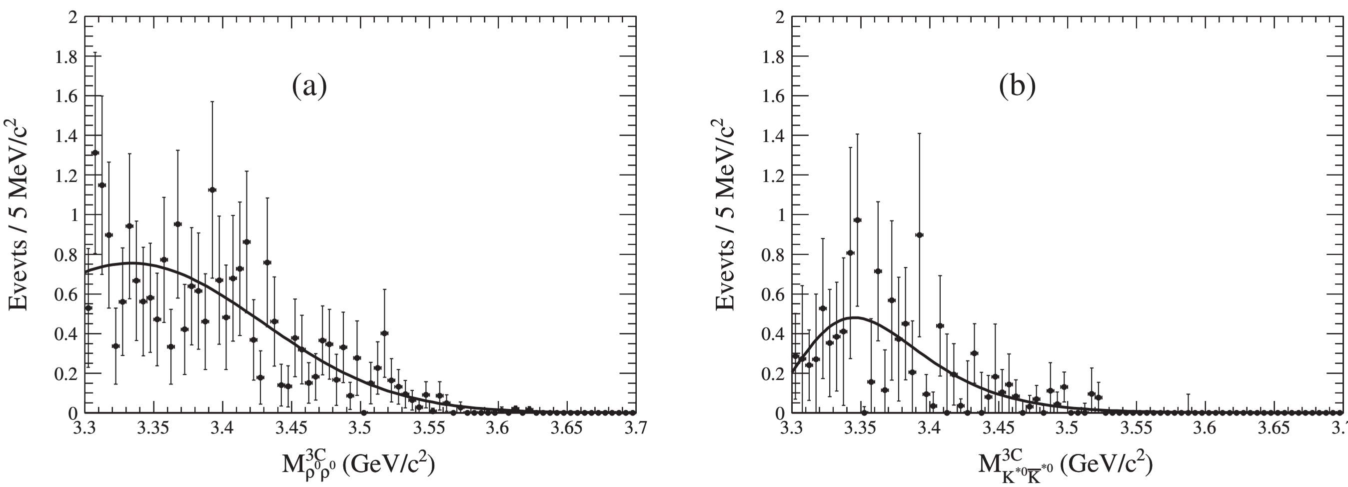

FIG. 2. The measured background from $\psi' \to \pi^0 X$ events (dots with error bars) for the modes (a) $\gamma\rho^0\rho^0$ and (b) $\gamma K^{*0}\bar{K}^{*0}$. The curves show the best fit with Novosibirsk functions.

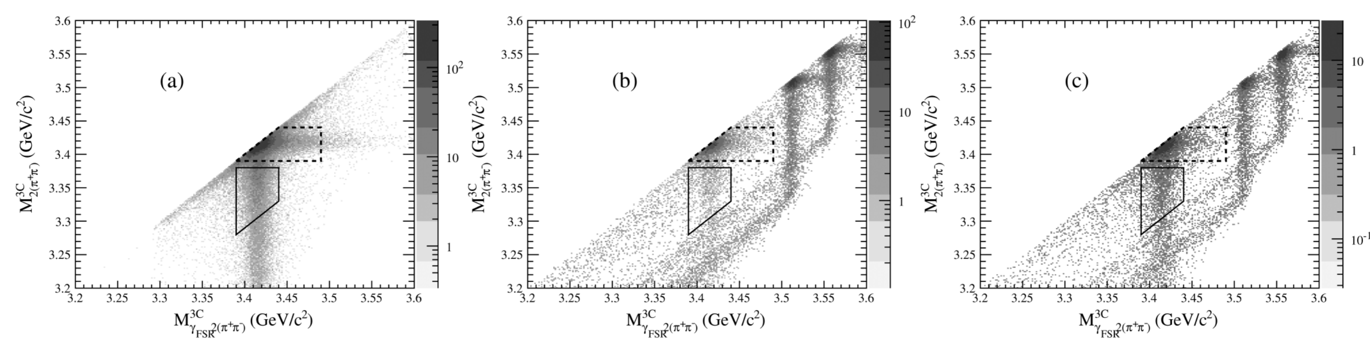

FIG. 3. The two-dimensional plots of M_X^{3C} versus $M^{3C}_{\gamma_{\rm FSR}X}$ for events passing the $\psi' \to \gamma\gamma_{\rm FSR}X$ selection with $X = 2(\pi^+\pi^-)$. From left to right they are (a) MC simulated χ_{c0} signal, (b) inclusive MC, and (c) data. In each plot the dashed-line and the solid-line boxes contain events without and with a FSR photon, respectively. MC simulations reproduce the shape well but not the amount of FSR events.

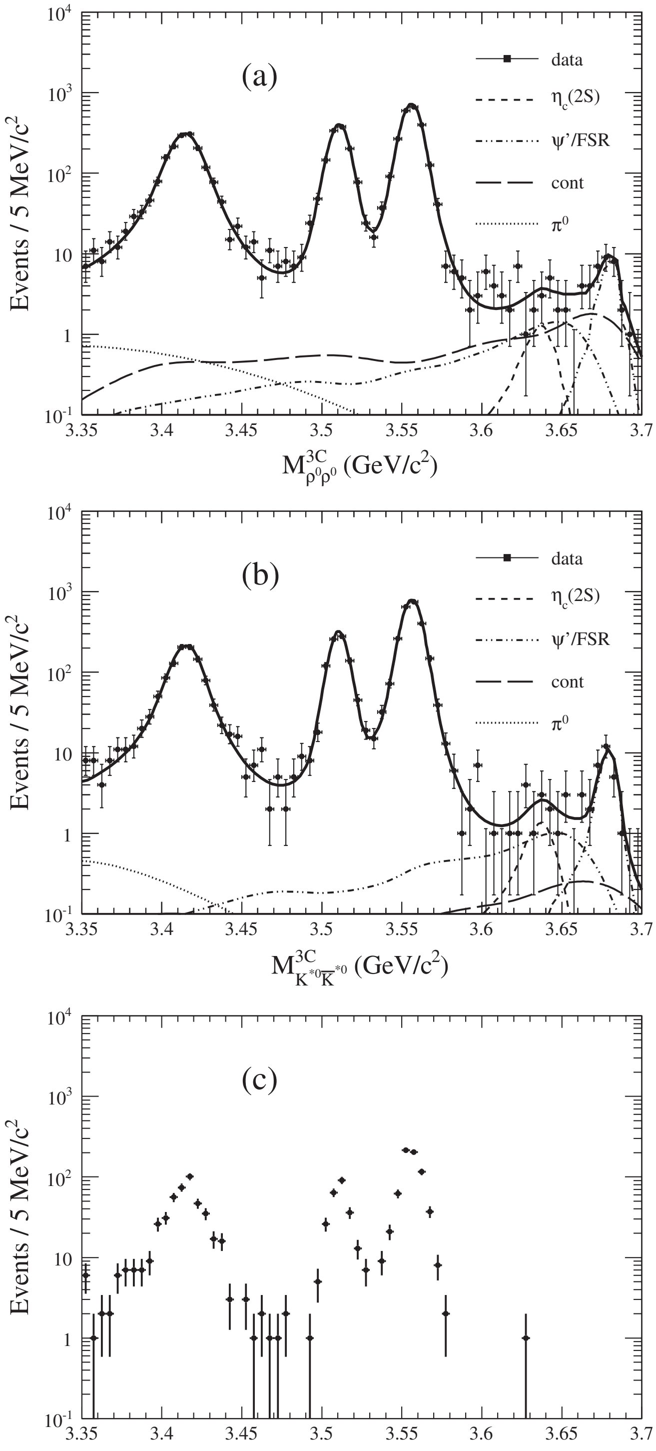

FIG. 4. Invariant mass distributions of the vector meson pairs after a $3C$ kinematic fit for the modes: (a) $\rho^0\rho^0$, (b) $K^{*0}\bar{K}^{*0}$, and (c) $\phi\phi$. Dots with error bars are data, and the solid curves in (a) and (b) are from the best fit to the mass spectra. No fit is performed for (c) due to low statistics. In (a) and (b), the η_c' signals are shown as short dashed lines, $\psi' \to \pi^0 X$ backgrounds are in dotted lines, continuum in long dashed lines, and $\psi' \to (\gamma_{\rm FSR})X$ in short dash-dot-dotted lines.

photon and X to calculate the invariant mass for events with M_X^{3C} below the χ_{c0} mass in the PDG ($M_{\chi_{c0}}^{\rm PDG}$), $M^{3C}_{\gamma_{\rm FSR}X}$ peaks at $M_{\chi_{c0}}^{\rm PDG}$ indicating the photon is indeed from FSR. As a result, events from $\chi_{c0} \to X$ are in the dashed-line box in Fig. 3, while events from $\chi_{c0} \to \gamma_{\rm FSR}X$ are in the solid-line box in Fig. 3. In this way, we can obtain $R_{\rm FSR}$ for MC simulation and data. The factor $f_{\rm FSR}$ is defined as the ratio of $R_{\rm FSR}$ measured in data to that determined in MC simulation. This FSR measurement is performed for two final states; $f_{\rm FSR} = 1.70 \pm 0.10$ and 1.39 ± 0.08 are determined for $X = 2(\pi^+\pi^-)$ and $X = \pi^+\pi^-K^+K^-$, respectively. The errors are the statistical errors of the sample and the uncertainties of the background estimation. These factors are used to scale fractions of FSR background events $[\psi' \to (\gamma_{\rm FSR})X]$ in the MC samples to estimate the background in data.

Data taken at $\sqrt{s} = 3.773$ GeV are used to estimate backgrounds from the continuum $[e^+e^- \to \gamma^* \to (\gamma_{\rm FSR})X]$ and initial state radiation ($e^+e^- \to \gamma_{\rm ISR}X$). MC simulation indicates that ψ'' decays contribute negligible background in the modes under study. Using the luminosity normalization and energy dependence of the cross section, there are 46 ± 3 and 8 ± 2 background events expected for $V = \rho^0$ and $V = K^{*0}$, respectively. For $V = \phi$, no events survive the selection.

The signal yields are extracted from an unbinned maximum likelihood fit to the M_{VV}^{3C} distribution. The signal shape is obtained from MC simulation, following $\mathrm{BW}(m_0, \Gamma) \times E_\gamma^3 \times \mathit{damping}$, where m_0 and Γ are the mass and width of the Breit-Wigner for signal and χ_{cJ}, E_γ^3 is the cube of the radiative photon energy, which is necessary in an $E1/M1$ radiative transition, and *damping* stands for a damping function used to damp the diverging tail caused by the E_γ^3 at lower mass region (corresponding to a higher energy radiative photon). One damping function used by the KEDR Collaboration [20] is defined as $\frac{E_0^2}{E_\gamma E_0 + (E_\gamma - E_0)^2}$, where E_0 is the most probable energy of the transition photon. It is also necessary to convolute this with a Gaussian function $G(\mu, \sigma)$ to take the mass

TABLE I. The systematic uncertainties in the measured product branching fraction $\mathcal{B}(\psi' \to \gamma\eta_c') \times \mathcal{B}(\eta_c' \to VV)$.

Source	ρ^0	K^{*0}	ϕ
Background (%)	14.9	9.9	0.0
Tracking (%)	8.0	8.0	8.0
Photon reconstruction (%)	1.0	1.0	1.0
Particle ID (%)	8.0	8.0	8.0
$4C$ fit (χ^2 selection) (%)	4.0	4.0	4.0
V mass selection requirement (%)	2.6	1.1	1.6
Damping function (%)	40.5	10.0	0.0
Mass and width of η_c' (%)	6.6	5.8	0.0
Number of ψ' (%)	4.0	4.0	4.0
Total (%)	45.6	19.9	12.8

TABLE II. From left to right, they are efficiency, upper limits at the 90% C.L. on the yield, product branching fraction $\mathcal{B}(\psi' \to \gamma\eta_c') \times \mathcal{B}(\eta_c' \to VV)$, η_c' decay branching fraction $\mathcal{B}(\eta_c' \to VV)$, and theoretical predictions from Ref. [6].

V	ε (%)	$N^{\rm up}_{\gamma VV}$	$\mathcal{B}^{\rm up}(\psi' \to \gamma\eta_c' \to \gamma VV)$ (10^{-7})	$\mathcal{B}^{\rm up}(\eta_c' \to VV)$ (10^{-3})	$\mathcal{B}^{\rm theory}(\eta_c' \to VV)$ (10^{-3})
ρ^0	14.3	19.2	12.7	3.1	6.4 to 28.9
K^{*0}	16.5	15.2	19.6	5.4	7.9 to 35.8
ϕ	19.9	3.9	7.8	2.0	2.1 to 9.8

resolution difference between MC simulation and data into account. The mean (μ) and standard deviation (σ) are free parameters for the χ_{cJ} signals. For η_c', they are fixed to the values extrapolated from χ_{cJ} with a linear assumption. In the fit, the estimated backgrounds from $\psi' \to \pi^0 X$ and the continuum are fixed. The shape of the $\psi' \to (\gamma_{\rm FSR})X$ background comes from the MC simulation. The fraction of MC data with an FSR photon is scaled by the factor $f_{\rm FSR}$ to estimate the fraction of data with FSR background. Figure 4 shows the final fitting results to the $3C$ mass spectrum. The values of χ^2/ndf are 0.68 and 0.72 for $\rho^0\rho^0$ and $K^{*0}\bar{K}^{*0}$, respectively, indicating good fits. The numbers of η_c' events obtained are 6.5 ± 6.4 and 6.9 ± 4.8 for $V = \rho^0$ and K^{*0}, respectively. No fit is performed for $\phi\phi$, since there is only one $\eta_c' \to \phi\phi$ candidate event in the signal region.

The systematic uncertainties related to tracking, photon reconstruction, PID and the kinematic fit are estimated with specially selected control samples [21]. An efficiency can be defined as the ratio of χ_{cJ} yield for VV with the V mass requirement to that without this requirement. The exact same method is applied to MC and the difference in the efficiency between MC simulation and data is taken as the corresponding systematic uncertainty caused by the V mass requirement, with the statistical error included. An alternative damping function was used by CLEO [22], $\exp(-E_\gamma^2/(8\beta^2))$, which is inspired by the overlap of wave functions, with $\beta = 65.0 \pm 2.5$ MeV from fitting the $J/\psi \to \gamma\eta_c$ photon spectrum. The difference caused by the two damping functions is taken as a systematic uncertainty. The main backgrounds that may affect our fit result in the η_c' mass region are the contributions from FSR in $\psi' \to \gamma_{\rm FSR}X$ and from the continuum. Therefore, the systematic uncertainty from the background shape is estimated by changing the FSR and continuum contributions by 1σ. There are also systematic uncertainties related to the mass and width of the η_c', which are estimated by comparing the η_c' yields with the mass and width fixed to the center values or randomly selected values according to a Gaussian distribution. Table I shows a summary of all the systematic uncertainties.

As there is no significant η_c' signal in any of the three final states, we determine upper limits on the $\psi' \to \gamma\eta_c' \to \gamma VV$ production rates. We assume all the signal events from the fit are due to $\eta_c' \to VV$, neglecting possible interference between the signal and nonresonant contributions. The probability density function (PDF) for the expected number of signal events is smeared with the systematic uncertainties (by convolution). For $V = \rho^0$ and K^{*0}, the PDF is taken to be the likelihood distribution in fitting the invariant mass distributions in Fig. 4 by setting the number of η_c' signal events from zero up to a very large number. For $V = \phi$, the one event in the η_c' mass region is taken as signal for simplicity, and the PDF is assumed to be a Poisson distribution.

The upper limit on the number of events at the 90% C.L., $N^{\rm up}_{\gamma VV}$, corresponds to $\int_0^{N^{\rm up}_{\gamma VV}} \mathrm{PDF}(x)dx / \int_0^\infty \mathrm{PDF}(x)dx = 0.90$ on the smeared PDF. The left half of Table II shows $N^{\rm up}$, the efficiencies from MC simulation, and the upper limits on the product branching fraction $\mathcal{B}(\psi' \to \gamma\eta_c') \times \mathcal{B}(\eta_c' \to VV)$. Using $\mathcal{B}(\psi' \to \gamma\eta_c') = (4.7 \pm 0.9 \pm 3.0) \times 10^{-4}$ [4], the corresponding upper limits on $\mathcal{B}(\eta_c' \to VV)$ are listed in the right half of Table II. In calculating $\mathcal{B}^{\rm up}(\eta_c' \to VV)$, the error on $\mathcal{B}(\psi' \to \gamma\eta_c')$ is taken as a systematic uncertainty to smear the PDF. The theoretical predictions [6] on branching fractions for $\eta_c' \to VV$, which are calculated with $\Gamma_{\eta_c'} = 10.4 \pm 4.2$ MeV [23], are also listed in Table II.

In conclusion, no obvious η_c' signal was observed in decays into vector meson pairs: $\rho^0\rho^0$, $K^{*0}\bar{K}^{*0}$, and $\phi\phi$. The upper limits on the product branching fraction $\mathcal{B}(\psi' \to \gamma\eta_c') \times \mathcal{B}(\eta_c' \to VV)$ and η_c' decay branching fraction $\mathcal{B}(\eta_c' \to VV)$ are determined. These upper limits are smaller than the lower bounds of the theoretical predictions [6], although the difference is very small for $\eta_c' \to \phi\phi$.

The BESIII Collaboration thanks the staff of BEPCII and the computing center for their hard efforts. This work is supported in part by the Ministry of Science and Technology of China under Contract No. 2009CB825200; National Natural Science Foundation of China (NSFC) under Contracts No. 10625524, No. 10821063, No. 10825524, No. 10835001, No. 10935007; the Chinese Academy of Sciences (CAS) Large-Scale Scientific Facility Program; CAS under Contracts No. KJCX2-YW-N29, No. KJCX2-YW-N45; 100 Talents Program of CAS; Istituto Nazionale di Fisica Nucleare, Italy; Siberian Branch of Russian Academy of Science, joint project No. 32 with CAS; U. S. Department of Energy under Contracts No. DE-FG02-04ER41291, No. DE-FG02-91ER40682, No. DE-FG02-94ER40823; University of Groningen (RuG) and the Helmholtzzentrum fuer Schwerionenforschung GmbH (GSI), Darmstadt; WCU Program of National Research Foundation of Korea under Contract No. R32-2008-000-10155-0.

[1] S. K. Choi *et al.* (Belle Collaboration), Phys. Rev. Lett. **89**, 102001 (2002).

[2] D. M. Asner *et al.* (CLEO Collaboration), Phys. Rev. Lett. **92**, 142001 (2004); B. Aubert *et al.* (*BABAR* Collaboration), Phys. Rev. Lett. **92**, 142002 (2004); B. Aubert *et al.* (*BABAR* Collaboration), Phys. Rev. D **72**, 031101 (2005).

[3] A. Vinokurova *et al.* (Belle Collaboration), arXiv:1105.0978v2; P. del Amo Sanchez *et al.* (*BABAR* Collaboration), Phys. Rev. D **84**, 012004 (2011); H. Nakazawa (Belle Collaboration), Proc. Sci., ICHEP2010 (2010) 162.

[4] L. L. Wang for the BESIII Collaboration, *XIV International Conference on Hadron Spectroscopy, 2011, Munchen, Germany*, arXiv:1110.2560.

[5] S. J. Brodsky and G. P. Lepage, Phys. Rev. D **24**, 2848 (1981); V. L. Chernyak and A. R. Zhitnitsky, Nucl. Phys. **B201**, 492 (1982); Phys. Rep. **112**, 173 (1984).

[6] Q. Wang, X. H. Liu, and Q. Zhao, arXiv:1010.1343.

[7] X. H. Liu and Q. Zhao, Phys. Rev. D **81**, 014017 (2010); J. Phys. G **38**, 035007 (2011).

[8] Q. Zhao *et al.*, Chinese Phys. C **34**, 299 (2010); Q. Zhao, Nucl. Phys. B, Proc. Suppl. **207-208**, 347 (2010).

[9] X. H. Mo, C. Z. Yuan, and P. Wang, High Energy Phys. Nucl. Phys. **31**, 686 (2007) [arXiv:hep-ph/0611214].

[10] M. Ablikim *et al.* (BESIII Collaboration), Phys. Rev. D **81**, 052005 (2010).

[11] M. Ablikim *et al.* (BESIII Collaboration), Nucl. Instrum. Methods Phys. Res., Sect. A **614**, 345 (2010).

[12] S. Agostinelli *et al.*, Nucl. Instrum. Methods Phys. Res., Sect. A **506**, 250 (2003).

[13] J. C. Chen, G. S. Huang, X. R. Qi, D. H. Zhang, and Y. S. Zhu, Phys. Rev. D **62**, 034003 (2000).

[14] K. Nakamura *et al.* (Particle Data Group), J. Phys. G **37**, 075021 (2010).

[15] The amplitudes and phases for H + , H0, and H- are 1.0, 0.0, 0.0, 0.0, -1.0, 0.0, which are calculated by requiring of P-parity conservation for the allowed components of helicity amplitudes.

[16] D. J. Lange, Nucl. Instrum. Methods Phys. Res., Sect. A **462**, 152 (2001).

[17] The $\pi^+\pi^-$ recoil mass is defined as $M_{\pi^+\pi^-}^{\mathrm{recoil}} = \sqrt{(E_{\psi'} - E_{\pi^+} - E_{\pi^-})^2 - (\vec{p}_{\psi'} - \vec{p}_{\pi^+} - \vec{p}_{\pi^-})^2}$, where E and $\vec{p}$ are energy and momentum for a particle.

[18] The Novosibirsk function is defined as $f(m_{ES}) = A_S \exp(-0.5\ln^2[1 + \Lambda\tau \cdot (m_{ES} - m_0)]/\tau^2 + \tau^2)$, where $\Lambda = \sinh(\tau\sqrt{\ln 4})/(\sigma\tau\sqrt{\ln 4})$, the peak position is m_0, the width is σ, and τ is the tail parameter.

[19] E. Barberio and Z. Was, Comput. Phys. Commun. **79**, 291 (1994).

[20] V. V. Anashin *et al.*, arXiv:1012.1694.

[21] M. Ablikim *et al.* (BESIII Collaboration), Phys. Rev. D **83**, 112005 (2011); Phys. Rev. Lett. **107**, 092001 (2011).

[22] R. E. Mitchell *et al.* (CLEO Collaboration), Phys. Rev. Lett. **102**, 011801 (2009); R. E. Mitchell *et al.* (CLEO Collaboration), Phys. Rev. Lett. **106**, 159903 (2011).

[23] By averaging measurements listed by the PDG [14] and recent results from *BABAR* and Belle, we determine the mass $M_{\eta_c'} = 3637.7 \pm 1.3\ \mathrm{MeV}/c^2$, and the width $\Gamma_{\eta_c'} = 10.4 \pm 4.2$ MeV